Journal of Controlled Release 293 (2019) 183–192

Contents lists available at ScienceDirect

Journal of Controlled Release

journal homepage: www.elsevier.com/locate/jconrel

Cabazitaxel-loaded Poly(2-ethylbutyl cyanoacrylate) nanoparticles improve treatment efficacy in a patient derived breast cancer xenograft

Markus Fusser[a], Anders Øverbye[b,1], Abhilash D. Pandya[a,1], Ýrr Mørch[c], Sven Even Borgos[c], Wanja Kildal[d], Sofie Snipstad[c,e], Einar Sulheim[c,e], Karianne Giller Fleten[a], Hanne Arenberg Askautrud[d], Olav Engebraaten[a,f], Kjersti Flatmark[a,f], Tore Geir Iversen[b], Kirsten Sandvig[b,g], Tore Skotland[b,*,1], Gunhild M. Mælandsmo[a,h,1]

[a] Department of Tumor Biology, Institute for Cancer Research, The Norwegian Radium Hospital, Oslo University Hospital, Oslo, Norway
[b] Department of Molecular Cell Biology, Institute for Cancer Research, The Norwegian Radium Hospital, Oslo University Hospital, Oslo, Norway
[c] Department of Biotechnology and Nanomedicine, SINTEF AS, Trondheim, Norway
[d] Institute for Cancer Genetics and Informatics, The Norwegian Radium Hospital, Oslo University Hospital, Oslo, Norway
[e] Department of Physics, The Norwegian University of Science and Technology, Trondheim, Norway
[f] Institute for Clinical Medicine, The Medical Faculty, University of Oslo, Oslo, Norway
[g] Department of Biosciences, University of Oslo, Oslo, Norway
[h] Department of Pharmacy, University of Tromsø, Tromsø, Norway

ARTICLE INFO

Keywords:
Poly(alkyl cyanoacrylate) nanoparticles
Breast cancer
Cabazitaxel
Biodistribution
Macrophage infiltration
Cell toxicity

ABSTRACT

The effect of poly(2-ethyl-butyl cyanoacrylate) nanoparticles containing the cytotoxic drug cabazitaxel was studied in three breast cancer cell lines and one basal-like patient-derived xenograft model grown in the mammary fat pad of immunodeficient mice. Nanoparticle-encapsulated cabazitaxel had a much better efficacy than similar concentrations of free drug in the basal-like patient-derived xenograft and resulted in complete remission of 6 out of 8 tumors, whereas free drug gave complete remission only with 2 out of 9 tumors. To investigate the different efficacies obtained with nanoparticle-encapsulated versus free cabazitaxel, mass spectrometry quantification of cabazitaxel was performed in mice plasma and selected tissue samples. Nanoparticle-encapsulated drug had a longer circulation time in blood. There was approximately a three times higher drug concentration in tumor tissue 24 h after injection, and two times higher 96 h after injection of nanoparticles with drug compared to the free drug. The tissue biodistribution obtained after 24 h using mass spectrometry analyses correlates well with biodistribution data obtained using IVIS® Spectrum in vivo imaging of nanoparticles labeled with the fluorescent substance NR668, indicating that these data also are representative for the nanoparticle distribution. Furthermore, immunohistochemistry was used to estimate infiltration of macrophages into the tumor tissue following injection of nanoparticle-encapsulated and free cabazitaxel. The higher infiltration of anti-tumorigenic versus pro-tumorigenic macrophages in tumors treated with the nanoparticles might also contribute to the improved effect obtained with the nanoparticle-encapsulated drug. Tumor infiltration of pro-tumorigenic macrophages was four times lower when using nanoparticles containing cabazitaxel than when using particles without drug, and we speculate that the very good therapeutic efficacy obtained with our cabazitaxel-containing particles may be due to their ability to reduce the level of pro-tumorigenic macrophages in the tumor. In summary, encapsulation of cabazitaxel in poly(2-ethyl-butyl cyanoacrylate) nanoparticles seems promising for treatment of breast cancer.

Abbreviations: AUC, Area under the curve; CBZ, cabazitaxel; EPR, enhanced permeability and retention; i.v., intravenously; LC, liquid chromatography; LNs, lymph nodes; LOQ, limit of quantification; PACA, poly(alkyl cyanoacrylate); PBCA, poly(n-butyl cyanoacrylate); PDI, polydispersity index; PDX, patient-derived xenograft; PEBCA, poly(2-ethyl-butyl cyanoacrylate); PEG, polyethylene glycol; POCA, poly(octyl cyanoacrylate); MS, mass spectrometry; NPs, nanoparticles; TAMs, tumor-associated macrophages.

* Corresponding author.
E-mail address: torsko@rr-research.no (T. Skotland).
[1] Equal contribution.

https://doi.org/10.1016/j.jconrel.2018.11.029
Received 28 May 2018; Received in revised form 28 November 2018; Accepted 30 November 2018
Available online 04 December 2018

1. Introduction

Chemotherapy has during recent years improved the treatment and prognosis of different cancers, but the therapeutic effect is not sufficient for certain cancer types and the treatment may also result in unwanted side effects. Several products of drug-loaded NPs have reached the market, and many new product candidates are in clinical trials. These aspects, including the challenges and opportunities of using nanoparticles in cancer drug delivery, have been discussed in several reviews [1,2]. In addition to improving efficacy by benefiting from the enhanced permeability and retention (EPR) effect [3], NP encapsulated drug delivery may demonstrate reduced toxicity. The main advantage of the drug-loaded NPs that have reached the market is that they give less adverse effects than free drug, while the therapeutic efficacy is rather similar [4].

Poly(alkyl cyanoacrylate) (PACA) was first developed and approved as surgical glue, and has later demonstrated promising abilities as a drug carrier, being biodegradable and allowing high drug loading capacity [5]. We have earlier shown that the degradation rate of PACA NPs can be controlled by the choice of the alkyl chain of the cyanoacrylate monomer [6], and we recently demonstrated, using a panel of cell lines, that the cytotoxicity was dependent on the monomers used, i.e. n-butyl-, 2-ethyl-butyl-, or octyl cyanoacrylate (PBCA, PEBCA and POCA, respectively) [7]. Based on this experience the present study was initiated to evaluate the effect of PEBCA NPs in breast cancer.

The PEBCA NPs used in this study contain the cytotoxic drug cabazitaxel (CBZ), a semi-synthetic taxane derivative which inhibits microtubule disassembly [8]. CBZ is approved by the US Food and Drug Administration (FDA) for treatment of refractory prostate cancer as a second line drug after docetaxel chemotherapy [9,10]. One advantage of CBZ is its low affinity for P-glycoprotein, thus reducing the possibility of obtaining drug resistance [8,11]. The very low water solubility of CBZ complicates administration of the free drug. However, the excellent compatibility and solubility of CBZ in alkyl cyanoacrylate monomer solution allows for encapsulation of high concentrations of the drug in PACAs. The NPs were surface modified with the polyethylene glycol (PEG)-containing molecules Pluronic F68 and Kolliphor HS15 to obtain an increased circulation time after intravenous (i.v.) injection [12].

Breast cancer can be classified into major subgroups based on the gene expression pattern. Tumors belonging to the most aggressive subtypes are commonly treated with antracycline- and taxane-based chemotherapy regimens. In particular, for hormone receptor and HER2 negative (often basal-like) tumors no targeted therapies are available, and the patients would therefore benefit from improved chemotherapy regimens [13]. One strategy may be to use NPs as encapsulation of doxorubicine in liposomes has been reported to increase drug uptake into breast cancer [14,15]. In the current study, the growth inhibitory effect of CBZ encapsulated into PEBCA NPs was evaluated in breast cancer models in vitro and in vivo. Three breast cancer cell lines representing the two main types of breast cancer, the luminal and basal-like subgroups, were used. One of the cell lines was also injected and grown in the mammary fat pad of immunodeficient mice. Additionally, one patient-derived xenograft (PDX) model previously demonstrated to be triple negative and representative for aggressive basal like breast cancer [16] was included in the study.

The main finding is the improved therapeutic effect of PEBCA-CBZ compared to free CBZ (i.e. the Jevtana® formulation) demonstrated in the basal-like PDX model. Immunohistochemical staining revealed a lower content of pro-tumorigenic macrophages in the PEBCA-CBZ treated tumors than in tumors treated with free CBZ, which may partly explain the improved efficacy. To elucidate the difference in efficacy of PEBCA-CBZ and free CBZ, we also showed in vivo biodistribution of particles loaded with the lipophilic fluorescent substance NR668. Furthermore, we used quantitative LC-MS/MS analyses to describe the biodistribution of CBZ in tissues and the kinetics of CBZ in blood plasma after injection of both PEBCA-CBZ and free CBZ.

2. Materials and methods

2.1. Synthesis and characterization of nanoparticles

PEGylated PEBCA NPs were synthesized by miniemulsion polymerization. An oil phase consisting of 2.5 g 2-ethylbutyl cyanoacrylate (monomer, Cuantum Medical Cosmetics, Spain) containing 0.2% (*w*/w) butylated hydroxytoluene (Fluka, Switzerland), and 2% (*w*/w) Miglyol 812 (Cremer, USA) was prepared. Fluorescent particles for optical imaging were prepared by adding NR668 (modified Nile Red) [17], custom synthesis, 0.2% (*w*/w) to the oil phase. Particles containing cytostatic drug for treatment were prepared by adding CBZ (10% (*w*/w), Biochempartner Co. Ltd., China, product item number BCP02404) to the oil phase, whereas vanillin (10% (w/w), Sigma-Aldrich, France) was used as an inert model drug in control particles.

An aqueous phase consisting of 0.1 M HCl (20 ml) containing Pluronic F68 (2 mM, Sigma, USA) and Kolliphor HS15 (6 mM, Sigma, Germany) was added to the oil phase and immediately sonicated for 3 min on ice (6 × 30 *sec* intervals, 60% amplitude, Branson Ultrasonics digital sonifier 450, USA). The solution was rotated (15 rpm, SB3 rotator, Stuart, UK) at room temperature overnight before adjusting the pH to 5 using 1 M NaOH. The polymerization was continued for 5 h at room temperature on rotation. The dispersion was dialyzed (Spectra/Por dialysis membrane MWCO 100,000 Da, Spectrum Labs, USA) against 1 mM HCl to remove unreacted PEG. The size, polydispersity index (PDI) and the zeta potential of the NPs were measured by dynamic light scattering and laser Doppler Micro-electrophoresis using a Zetasizer Nano ZS (Malvern Instruments, UK). To calculate the amount of encapsulated drug, the drug was extracted from the particles by dissolving them in acetone (1:10), and quantified by liquid chromatography coupled to mass spectrometry (LC-MS/MS) as described below.

2.2. CBZ quantification by LC-MS/MS

CBZ, as the pure chemical or part of NPs, was quantified by LC-MS/MS, using an Agilent 1290 HPLC system coupled to an Agilent 6490 triple quadrupole mass spectrometer. The HPLC column was an Ascentis Express C8, 75 × 2.1 mm, 2.7 μm particles size with a 5 × 2.1 mm guard column of the same material (Sigma), run at 40 °C. Eluent A was 25 mM formic acid in water and eluent B was 100% methanol, and flow rate was 0.5 ml/min. The mobile phase gradient was isocratic at 55% B for 1.5 min, then from 55% to 80% B over 1 min, followed by 1 min washout time and subsequently column re-equilibration. Injection volume was 5.00 μl. MS detection was in positive ESI mode (Agilent Jetstream) quantified in multiple reaction monitoring (MRM) mode using the transition *m/z* 858.3 → 577.2. The parent ion was chosen to be the Na adduct as this gave the best sensitivity. Similarly, the hexadeuterated internal standard was detected on the 864.4 → 583.2 transition. Both analytes were run at 380 V fragmentor and 20 V collision energy.

Reference standards were used for accurate quantification. The unlabeled CBZ standard was the same as used for synthesis (see above) at > 98% purity. Hexadeuterated CBZ internal standard was purchased from Toronto Research Chemicals (Toronto, Canada; catalogue number C046502 at 99.6% isotopic purity). Standards were dissolved in acetone and were used to build an unlabeled standard series spanning at least five concentration points

The limit of quantification (LOQ) was calculated from six replicate quantifications of the lowest concentration point in the standard curves (0.1 ng/ml), specifically as the average plus six standard deviations; this amounted to an LOQ of 0.19 ng/ml (signal/noise ratio >20). Accuracy based on the same standard sample set was 8.8% and precision was 18.0%.

2.3. Processing of tissue samples before LC-MS/MS analyses

In order to process the tissue samples such that their CBZ content could be quantified, we developed a protocol for enzymatic digestion of tissue followed by extraction and quantification of CBZ using the LC-MS/MS method described above. The enzyme buffer consisted of Dulbecco's Modified Eagle Medium (DMEM, Thermo Fisher Scientific, USA, 41965039) with 1% (*v*/v) penicillin-streptomycin stock solution (Sigma-Aldrich, P0781) to a final concentration of 100 U/ml penicillin and 100 µg/ml streptomycin, 0.125 mg/ml papain (Merck, F275644), 2.5 mg/ml trypsin (Sigma-Aldrich, T7409), 0.8 mg/ml collagenase (Sigma-Aldrich, C7926), 0.69 mg/ml hyaluronidase (Sigma-Aldrich, H3506) and 1% (*v*/v) Triton X-100 (Sigma-Aldrich, T-8787). To determine the biodistribution of CBZ, frozen organs (liver, spleen, lymph nodes, kidneys, tumors) were thawed and freshly prepared enzyme buffer was added at 1 ml per 50 mg tissue; the entire organs were digested. The samples were heated to 37 °C for 72 h with vortexing once a day, until the tissue was completely dissolved. Stability of CBZ under these conditions was verified by incubation of known concentrations of the free drug. The tissue digests, as well as the plasma samples from the animals, were diluted 10× in acetone before centrifugation; this has the dual effect of both precipitating proteins and other macromolecules, thus cleaning up the sample, and making sure all cabazitaxel is solubilized. Internal standard (hexadeuterated CBZ) dissolved in acetone was added to a final concentration of 10 ng/ml during the acetone dilution to correct for possible matrix effects.

2.4. Cell lines

Three commonly used breast cancer cell lines [18] were used. The MDA-MB-231, (triple negative; Claudin low), was cultured in RPMI 1640; the MDA-MB-468 (triple negative; basal) and the MCF-7 (luminal A) [18] cell lines were cultured in DMEM. All medium was fortified with 10% (*w/v*) fetal calf serum albumin (Sigma) and 100 units/ml penicillin/streptomycin (PenStrep®, Sigma). All cell lines were obtained from ATCC and were routinely tested for mycoplasma. Cells growing in 24- or 96-well plates were incubated with serial dilutions of PEBCA-CBZ, CBZ (non-encapsulated CBZ) dissolved in Tween-80 (Fluka)), and PEBCA without CBZ for 24, 48 or 72 h at 37 °C in an atmosphere of 5% CO_2. The toxicity was assessed either by the commonly used MTT (3-(4,5-dimethylthiazol-2-yl)-2,5-diphenyltetrazolium bromide) cell viability assay, by measuring cell proliferation based on [^{3}H]thymidine incorporation, by measuring protein synthesis by incorporation of [^{3}H] leucine and by measuring ATP levels using CellTiter Glo® .

2.5. MTT cell viability assay

The cells were incubated for 24, 48 and 72 h with the different NPs/substances. The cell medium was then aspirated and exchanged with 100 µl of medium containing a final concentration of 250 µg MTT/ml. The incubation was continued for 3 h at 37 °C for formation of the formazan-particles, which were dissolved in DMSO with 1% (*v*/v) NH_4Cl. The absorbance was read in a plate reader (Biosys Ltd., Essex, UK) at 570 nm, and background from absorbance at 650 nm was subtracted.

2.6. Cell proliferation measured by [^{3}H]thymidine incorporation

Incorporation of [^{3}H]thymidine into DNA was used to estimate cell proliferation. The cells were incubated for 24 h with the different NPs/substances. The cell medium was then aspirated and substituted with serum free cell medium containing [^{3}H]thymidine (3 µg/ml; 75 µCi/ml). The incubation was continued for 30 min at 37 °C. The medium was removed and 5% (*w/v*) trichloroacetic acid (TCA) was added. After 5 min the cells were washed twice with TCA and solubilized with 200 µl of 0.1 M KOH, before mixing with 3 ml scintillation fluid (Perkin Elmer, USA). The radioactivity was counted for 1 min in a scintillation counter (Tri-Carb 2100TR, Packard Bioscience, USA).

2.7. Protein synthesis measured by [^{3}H]leucine incorporation

To determine the impact of PEBCA-CBZ and CBZ on protein synthesis, the cells were incubated with these substances for 24 h. The cell medium was then aspirated, the cells washed once with leucine-free HEPES medium (28 mM HEPES, (4-(2-hydroxyethyl)-1-piperazineethanesulfonic acid) in MEM) and further incubated with leucine-free HEPES medium containing [^{3}H]leucine (2 µCi/ml) for 30 min at 37 °C. The medium was removed and 5% (*w/v*) TCA was added to precipitate proteins. After 5 min the cells were washed again with 5% (w/v) TCA and solubilized with 200 µl of 0.1 M KOH, before mixing with 3 ml scintillation fluid and counting the radioactivity as described above.

2.8. Cell viability estimated by measuring ATP

Viability of the cells was tested measuring the ATP levels by using the CellTiter-Glo® (Promega,WI, USA) assay, as described by the supplier. Cells were incubated with PEBCA-CBZ or CBZ for 72 h, thereafter one half of the volume was removed, replaced with an equal volume of the ATP reagent and gently mixed. After incubation for 10 min the cell lysate was transferred to a light-protected 96-well plate and luminescence measured in a plate reader (Biosys Ltd., Essex, UK).

2.9. Treatment efficacy evaluation in nude mice

All animal experiments were approved and performed according to the Norwegian Animal Research Authority (Permit number 15-136041) and were conducted according to the regulations of the Federation of European Laboratory Animal Science Association (FELASA). The mice were kept under pathogen-free conditions, at constant temperature (21.5 ± 0.5 °C) and humidity (55 ± 5%); 15 air changes/h and a 12 h light/dark cycle. They had access to distilled water ad libitum, which was supplemented with 17-β-estradiol at a concentration of 4 mg/l [19]. All mice used in this study were female athymic nude *foxn1^{nu}* mice (age 5–6 weeks and body weights of 18–20 g), locally bred at the Department of Comparative Medicine, Oslo University Hospital, Norway. In all procedures where anesthesia was required 4% sevofluran was used.

The orthotopically growing basal-like xenograft MAS98.12 has been established in house [19] and was used as previously described [16]. When using the MDA-MB-231 cell line, 1.5 million cells were injected into the mammary fat pad and growing tumors were used for sequential implantation. As for the MAS98.12 model, 1–2 mm^3 pieces of healthy tumor tissue were implanted bilaterally into the mammary fat pad of female athymic mice. After the tumors reached approximately 5 mm in diameter, the mice were randomly assigned to the different treatment groups (the average volume of each group was 49–57 mm^3).

All formulations were given twice (day 1 and day 4 after randomization) as i.v. tail vein injections. PEBCA-CBZ NPs were given with a dose of CBZ 15 mg/kg and comparable amount of empty PEBCA NPs (175 mg/kg) as control. Non-encapsulated cabazitaxel was prepared as a stock solution in Polysorbate 80 (40 mg/ml) and further diluted with 13% (*v*/v) ethanol to a working solution of 10 mg/ml CBZ. The injection solution was prepared directly before the administration by dilution of the working solution with 0.9% (*w/v*) NaCl. The same amount of ethanol (1.2–1.4% (v/v)) was used as vehicle control; injection volumes were in the range 200–290 µl. From the first day of treatment, tumor diameter and body weight were measured twice weekly. Mice were monitored daily for health status and were killed by cervical dislocation if they became moribund or if tumor reached 1500 mm^3. The tumor was measured by calipers and the tumor volume was calculated according to the formula 0.5 x length x width^2 and related to the tumor volume at

start of treatment.

2.10. In vivo imaging

PEBCA NPs labeled with the lipophilic and fluorescent dye NR668 were used to study the biodistribution in MA98.12 bearing mice using an IVIS® Spectrum in vivo imaging system (Perkin Elmer). Mice were intravenously injected the same single dose PEBCA-CBZ or PEBCA without drug as in the efficacy study. The batch containing CBZ has somewhat larger particles than the batch not containing CBZ (Table S1). The excitation/emission wavelength pair of 535/640 nm was found to give the best signal-to-noise ratio and was thus used for imaging of the NPs. Whole body images were obtained 1, 4, 24 and 96 h after injection; the animals were then sacrificed by cervical dislocation and organs were harvested. The organs were imaged ex vivo with the IVIS scanner using the same settings as above. Relative signal intensity in the organs was calculated, using Living Image software (Perkin Elmer), as radiant efficiency (Emission light [photons/s/cm^2/str]/ Excitation light [μW/cm^2] × 10 [9]) per pixel of the region of interest, which was drawn around the respective organ. Fluorescent measurements of the PEBCA NPs used for in vivo imaging showed that the particles without CBZ had a fluorescent intensity of 1.17 times that of the PEBCA NPs containing CBZ and the data shown in Fig. 3C are corrected for this difference.

2.11. Biodistribution and pharmacokinetics in blood

Blood and tissue samples were obtained following a single i.v. injection of PEBCA-CBZ and non-encapsulated CBZ (15 mg/kg) into the tail vein of mice bearing the MAS98.12 tumor (n = 3). Empty particles (PEBCA) and saline were used as negative controls. The blood samples were taken either per tail vein puncture (approximately after 2 min and thereafter at 1, 4 and 24 h after injection) or by terminal cardiac puncture (24 and 96 h after injection) in Vacutainer tubes containing EDTA (BD Biosciences, San Jose, CA, USA) and kept on ice. The 0–24 h samples were collected consecutively from the same animals (n = 3) while samples after 96 h were obtained from separate mice (n = 3). The blood was centrifuged for 15 min at 4 °C and 3400 x g, and the supernatant plasma was collected and stored at −80 °C until LC-MS/MS analysis. The animals were sacrified after 24 or 96 h and tissue samples (tumors, livers, spleens, lymph nodes and kidneys) were harvested. The organs were gently washed with saline and then snap frozen in liquid nitrogen and stored at −80 °C until further processing and LC-MS/MS analyses as described above. Statistical analyses were performed using the t-test.

2.12. Immunohistochemistry

Tumors from MAS98.12 bearing mice were collected 96 h after a single injection of the same substances as were injected in the MAS98.12 efficacy study. The tumors were preserved in 4% (v/v) formalin and then paraffinized and sliced to prepare consecutive slides (3 μm thick). The deparaffinization agent Neo-clear and mounting agent Neo-mount were obtained from VWR (Radnor, PA, USA). Heat induced epitope retrieval was performed by placing deparaffinized slides with 10 mM sodium citrate buffer (pH 6.0) in water bath for 20 min at 100 °C. Endogenous peroxidase activity was blocked by incubating slides with 3% (v/v) hydrogen peroxide in Tris-buffered saline (TBS; 50 mM Tris-Cl, 150 mM NaCl, pH 7.6). Sections were washed and blocking of non-specific binding was performed with 3% (w/v) bovine serum albumin (Roche diagnostics GmbH, Mannheim, Germany) in TBS for 30 min. Sections were then incubated for 60 min with the primary antibodies. Three different antibodies, i.e. anti-CD68 (1 mg/ml; ab125212, Abcam, Cambridge, UK), anti-CD206 (0.1 μg/ml; ab64693, Abcam, Cambridge, UK), and anti-iNOS (0.5 μg/ml; ab15323, Abcam, Cambridge, UK) were used to detect different populations of macrophages. CD68 is a commonly used marker for the whole macrophage population [20,21], iNOS (inducible nitric oxide synthase) is a marker for M1 macrophages (anti-tumorigenic and pro-inflammatory macrophages) [22], and CD206 is a marker for M2 macrophages (pro-tumorigenic and anti-inflammatory macrophages) [22]. TBS was used for washing the slides between steps. Detection of primary antibodies was performed using MACH 3 rabbit HRP-polymer detection kit according to the manufacturer's protocol (Biocare Medical, Concord, CA, USA). Signals were developed by incubation with the Chromogen solutions provided with the Betazoid DAB Chromogen kit (Biocare Medical). For counter staining a haematoxylin and 37 mM ammonium hydroxide containing solution (Sigma-Aldrich, St. Louis, MO, USA) were used.

Stained tissue sections were scanned (NanoZoomer HT, Hamamatsu Photonics, Hamamatsu, Japan) using a 40× objective. The extent of CD68, iNOS and CD206 was automatically scored using the ImmunoPath software (Room4 Ltd., Crowborough, UK) [23]. The tumor areas were marked manually, excluding necrotic areas as well as blood vessels to avoid unspecific or false positive staining. The annotated areas were then broken down to smaller frames per image of interest for efficient processing. The annotated representative areas were analyzed further by computerized image analysis. The image analysis protocols were set up on randomly selected images from different tumors to educate the software to differentiate between haematoxylin stained blue negative staining and brown positive staining. The output of the analysis provides the number of the positive pixel fraction and the negative pixel fraction of total annotated area of the whole tumors.

2.13. Statistical analyses

To calculate the significance in the efficacy studies, the area under the curve was calculated for each tumor and the mean values of the groups were compared using the Welch unequal variance. To determine whether there is a significant difference between the frequencies of the tumor regression in the different treatment groups, we used the Fischer's exact test. If not stated otherwise, an unpaired two-sided Student t-test without Welch correction was used. The statistical analyses were performed using either GraphPad Prism (version 7.00 for Windows, GraphPad Software, La Jolla, California, US) or Microsoft Excel.

3. Results

3.1. Characterization of PEBCA particles

The particle size, polydispersity index (PDI) and zeta potential for the batches used, were in the range of 148–227 nm (z-average), 0.04–0.19 and - (0.6–2.4) mV, respectively. The drug content in the final particles was 6.0–8.6% (w/w), giving 2.0–3.4 mg CBZ/ml in the NP stock solutions (Table S1). The size of PEBCA NPs increased when adding the drug CBZ (Table S1). The size distribution curves for the two batches used for efficacy studies in the MAS98.12 tumor model and that of CBZ (forming clusters in solution) are shown in Fig. 1.

3.2. PEBCA-CBZ inhibits tumor growth more efficiently than free CBZ in the MAS98.12 mice model

To test the efficacy of the PEBCA NPs with incorporated CBZ in a PDX model, MAS98.12 tumors were implanted into the mammary fat pad of nude mice and treated with the drug-loaded particles (PEBCA-CBZ), empty particles (PEBCA), non-encapsulated (free) CBZ and saline as control (Fig. 2A). The injected dose was 2 × 15 mg CBZ/kg body weight, which corresponds to a particle dose of 2 × 175 mg/kg (Fig. 2A). Tumor growth was not affected by empty PEBCA NPs, but markedly inhibited by CBZ. The effect was significantly more pronounced when the drug was encapsulated in the NPs compared to free

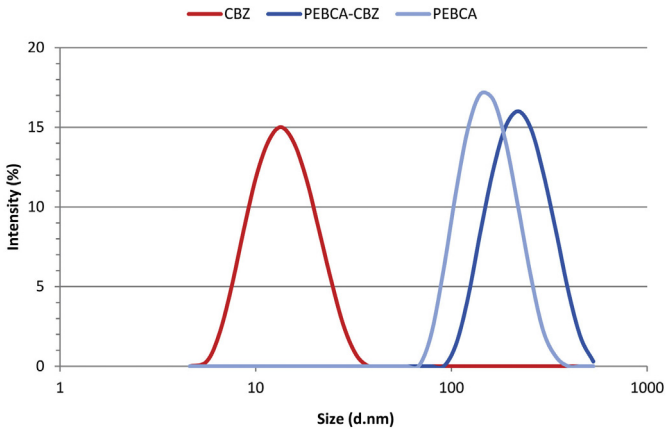

Fig. 1. Size distribution of the batches used in the MAS98.12 efficacy study. The size distributions for PEBCA-CBZ (the batch with size z-average of 215 nm in Table S1) is shown in dark blue and for PEBCA (without drug; the batch with z-average of 156 nm in Table S1) is shown in light blue. The size distribution of CBZ, which forms clusters in solution, is shown in red. Intensity (%) on the y-axis means percent intensity of the total scattered light. (For interpretation of the references to colour in this figure legend, the reader is referred to the web version of this article.)

drug (Fig. 2A). Notably, in the PEBCA-CBZ treated group 6 out of 8 tumors went into complete remission while this was the case in only 2 out of 9 CBZ-treated tumors and none in the negative control groups (Fisher's exact test (1-sided): p = 0.04; comparing PEBCA-CBZ with CBZ).

To further evaluate differences in tumor growth between the four groups, we calculated the area under the curve (AUC) for each individual tumor and compared the mean values of each treatment group. The efficacy of PEBCA-CBZ is significantly better than treatment with free CBZ (p = .02; Fig. S1). The toxicity of the different treatments measured as body weight relative to the weight at treatment start is shown in Fig. 2B. The two treatments with CBZ (non-encapsulated or encapsulated as PEBCA-CBZ) caused a decline in body weight by approximately 15%, but one week after the last injection the effect of the body weight was reversed. This tolerable body weight loss and the recovery time were comparable for PEBCA-CBZ and CBZ. Administration of empty PEBCA NPs did not cause any toxic effect as estimated from the body weights.

The efficacy of PEBCA-CBZ and non-encapsulated CBZ was also studied in MDA-MB-231 tumor-bearing mice. In this model we did not detect a significant difference between the two CBZ formulations, but a delay in tumor growth was observed (Fig. S2). When compared to MAS98.12, the CBZ (free and encapsulated drug) was less effective in the MDA-MB-231 tumors. It was not possible to improve the efficacy by increasing the dose, due to limiting systemic toxicity [8].

3.3. In vivo biodistribution of PEBCA particles

The biodistribution of the PEBCA NPs in MAS98.12 bearing mice was studied by fluorescence imaging up to 96 h after injection of particles containing the fluorescent dye NR668. The mice were imaged using the IVIS® Spectrum scanner after 1, 4, 24 and 96 h (Fig. 3A), and then sacrificed such that organs could be harvested and visualized ex vivo. The images of all organs harvested 24 h after injections are shown in Fig. 3B, and the mean radiant efficiency relative to the pixel size of the region of interest per organ is plotted in Fig. 3C. The images of organs obtained at 1, 4 and 96 h are shown in Fig. S3. Injection of the free NR668 dye did not give any detectable fluorescence with the wavelengths used (data not shown), thus indicating that the detected signals are from PEBCA-bound NR668. The images shown in Fig. 3 and Fig. S3 demonstrate a rapid uptake in all tissues shown; 24 h after injection the strongest signals were observed in liver, spleen and lymph nodes, although fluorescence also was easily detectable in tumors, kidneys, hearts and lungs (Fig. 3C).

3.4. Pharmacokinetics and biodistribution of encapsulated and non-encapsulated CBZ

PEBCA-CBZ and non-encapsulated CBZ (15 mg/kg) were intravenously (i.v.) injected into the tail vein of mice bearing the MAS98.12 tumor. Blood samples were taken approximately 2 min after injection, and 1, 4, 24 and 96 h after injection, and the plasma samples were analyzed for CBZ using an LC-MS/MS method. The CBZ concentrations at almost all time points were at least 10-fold higher in mice receiving PEBCA-CBZ compared to mice receiving free CBZ (Fig. 4A).

The plasma concentration/time curves for both PEBCA-CBZ and CBZ indicate an initial distribution phase, followed by a terminal elimination phase. The low number of data points did not allow determination of distribution or elimination half-life through non-linear regression. Interpolation based on the two first data points (up to 1 h) indicate distribution half-lives in the range of approximately 50 min and 30 min for PEBCA-CBZ and CBZ, respectively. Similarly, calculation of the elimination half-lives based upon the mean values of the two last time points (24 and 96 h) indicates half-lives of this phase of about 60 h for both compounds. The higher plasma concentration observed after administration of PEBCA-CBZ compared to CBZ suggests a lower distribution volume and lower total clearance for PEBCA-CBZ compared to CBZ. This is consistent with the NP formulation being less able to escape the vascular compartment, and elimination of NPs primarily through the reticuloendothelial system.

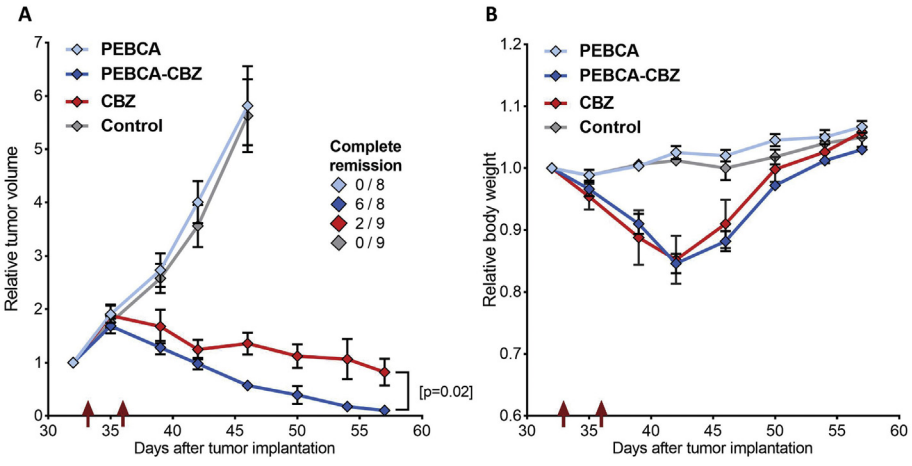

Fig. 2. Treatment efficacy and toxicity studied in mice bearing MAS98.12 PDX breast tumors. Tumor growth inhibition (A) and body weight change (B) after treatment. PEBCA-CBZ and CBZ were injected 2 × 15 mg CBZ/ kg body weight at day 33 and 36, indicated by the red arrows. Empty PEBCA NPs (same dose as PEBCA-CBZ) and saline were used as negative controls (mean ± SEM; n = 8–9 tumors/ 5–6 mice). Tumor size is relative to the size measured at time of randomization. Non-palpable tumors at day 57 after implantation are indicated as complete remissions. The statistical p-value of Welch t-test of areas under the curves is indicated (p = 0.02). (For interpretation of the references to colour in this figure legend, the reader is referred to the web version of this article.)

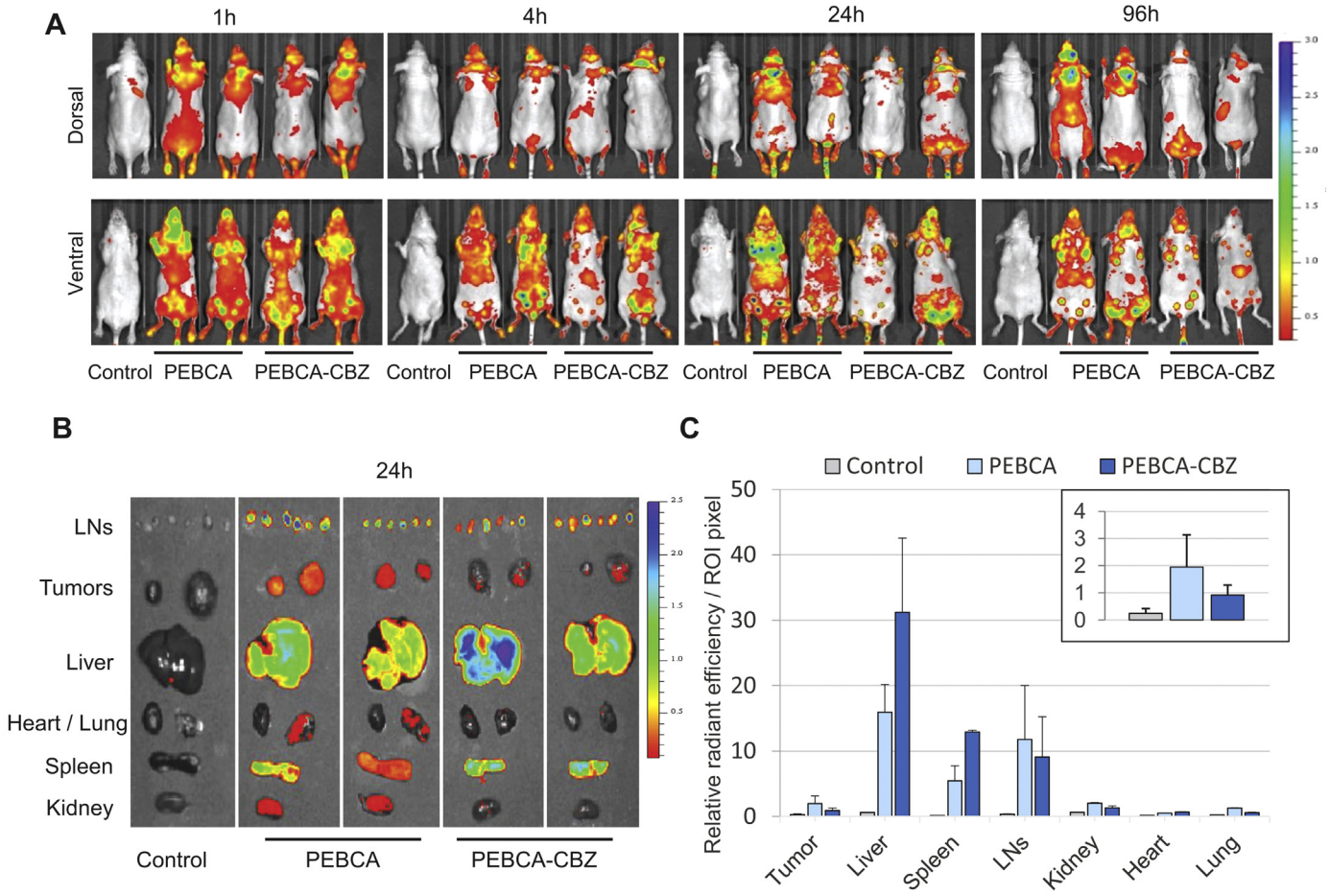

Fig. 3. Biodistribution of PEBCA particles containing the fluorescent dye NR668 measured in MAS98.12 tumor-bearing mice. Whole body images were obtained with IVIS 1, 4, 24 and 96 h after i.v. administration of the NPs; colour scale on the right indicates radian efficiency × 10^9 (A). Ex vivo fluorescence images of isolated organs were obtained 24 h after injection (B). Quantification of fluorescence intensity as relative radiant efficiency per region of interest pixel data of tissues collected 24 h after injection (C). Mean values obtained for 2 animals; error bars show SD values. PEBCA-CBZ: PEBCA containing CBZ and NR668; PEBCA: PEBCA containing NR668, but not CBZ. LNs: lymph nodes. The tumor data are enlarged in the inset.

The CBZ concentrations were measured in tumor, liver, spleen, lymph nodes, and kidney following a single injection of PEBCA-CBZ and CBZ (15 mg/kg). The results obtained with samples taken 24 and 96 h after injections are shown in Fig. 4B and C, respectively. The data are given as ng CBZ/mg tissue; for researchers wanting to have data as % ID/mg the injected dose was 0.27–0.30 mg CBZ. The highest amount of drug per mg tissue was obtained in spleen. However, when assuming that the mass of liver is approximately 13 times that of spleen in mice [24] the data in Fig. 4 indicates that the liver/spleen ratio of PEBCA-CBZ is 2.1 at 24 h after injection and 4.4 at 96 h after injection, demonstrating that liver is taking up the largest part of these NPs. The amounts of CBZ in the tumor samples measured as ng CBZ/mg tissue were 20% (24 h) and 1.4% (96 h) of that in liver after injection of PEBCA-CBZ.

The concentration of CBZ was significantly higher (*t*-test; *p*-value < .01) in all tissues analyzed at 24 h following injection of particle bound (PEBCA-CBZ) as compared to free drug (CBZ), with the largest differences observed in liver and spleen which contained the highest amounts of PEBCA-CBZ. In the samples obtained 96 h after injection, CBZ could be detected (i.e. being above the LOQ of the LC-MS/MS method; calculated to be 0.19 ng/ml) in all tissues analyzed after injection of PEBCA-CBZ. Following injection of free CBZ, the CBZ content was below the LOQ for all tissues except tumor tissue 96 h after injection, such that the CBZ content could be estimated in tumor tissue only (Fig. 4C). The CBZ content measured in tumors 24 h after injection of PEBCA-CBZ was approx. 1.2% of the injected dose. This was reduced to approx. 0.5% at 96 h after injection. The amount of CBZ found in tumors after injection of free CBZ was approximately half of that obtained after injection of PEBCA-CBZ at both time points. When comparing the CBZ concentrations in the tissue samples obtained 24 and 96 h after injection of PEBCA-CBZ, there is a decrease in tumor, spleen and kidney, and an increase in liver and lymph nodes from 24 to 96 h. The only significant difference is the decrease in the MAS98.12 tumor tissue ($p = .02$). Also, the CBZ concentration after injection of free CBZ was significantly lower in tumors after 96 h when compared to 24 h ($p < .001$). Plasma and tissue samples were also analyzed for CBZ following injection of PEBCA NPs without CBZ; all these samples (similar to those samples analyzed after injection of PEBCA-CBZ) were below the LOQ of the analytical method.

3.5. Macrophage infiltration in treated MAS98.12 tumors

The infiltration of CD68 antibody stained macrophages into control and treated MAS98.12 tumors was estimated using automatic quantification of scanned slides. An elevated number of tumor infiltrating macrophages was observed in mice injected with PEBCA-CBZ or PEBCA without drug compared to mice receiving free CBZ or saline, but the differences did not reach statistical significance (Fig. 5A). Also the marker of pro-inflammatory M1 macrophages (iNOS) demonstrated increased macrophage infiltration into tumors of mice receiving PEBCA-CBZ or PEBCA (Fig. 5B). However, the anti-inflammatory M2 macrophages subset, measured as CD206 positive cells, demonstrated

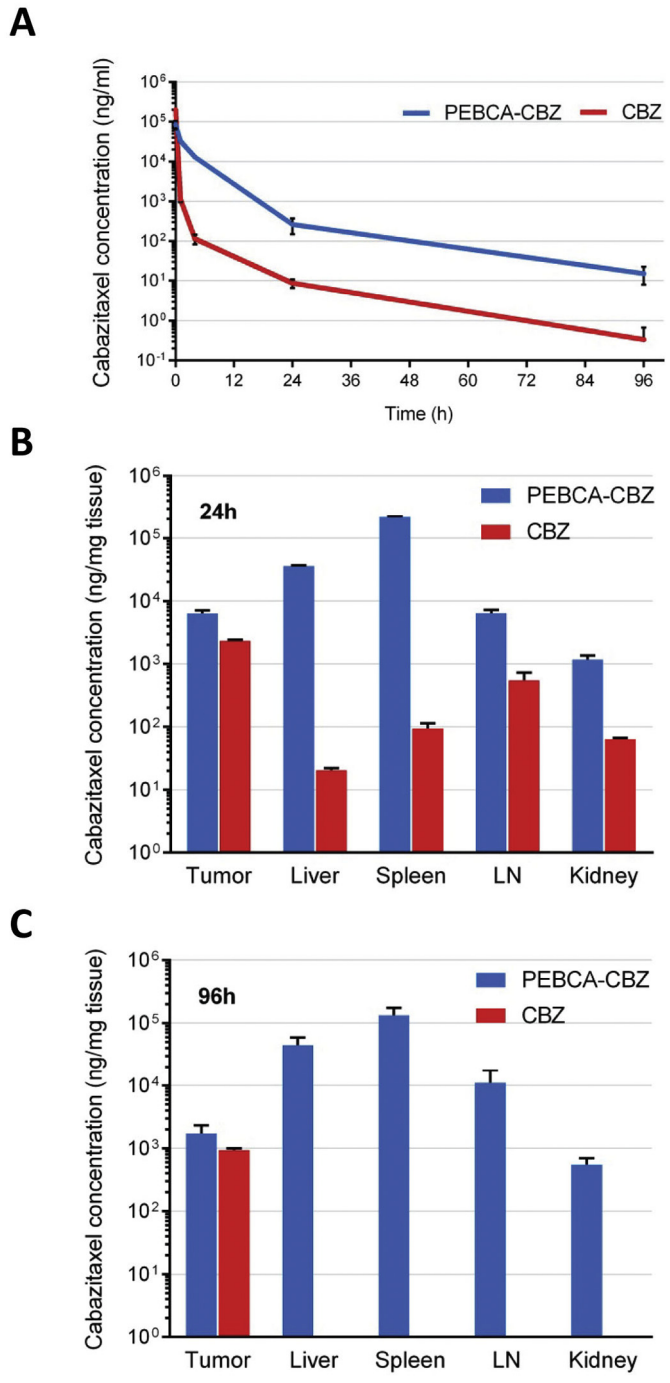

Fig. 4. CBZ concentrations in plasma and organs measured with LC-MS/MS after administration of 15 mg CBZ/kg. Plasma concentration measured as function of time (A). CBZ concentrations in tumors and organs measured after 24 h (B) and 96 h (C). LNs: lymph nodes. Data shown are mean values ± SD ($n = 3$). Note that logarithmic scales are used on all y-axes.

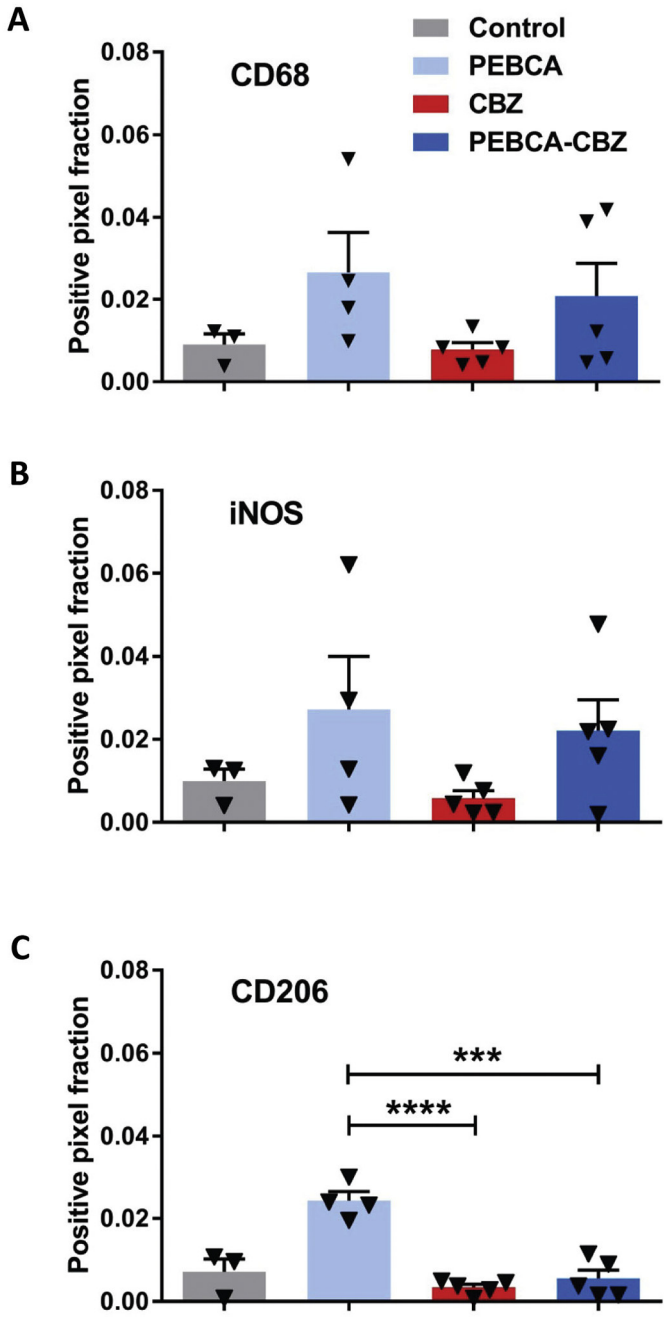

Fig. 5. Macrophage infiltration in treated MAS98.12 tumors. The macrophage infiltration was measured in the MAS98.12 tumors 96 h after injection of saline (control), PEBCA NPs (without drug), free CBZ, and PEBCA-CBZ. (A): The total population of infiltrated macrophages was quantified using an antibody to CD68. (B): The population of anti-tumorigenic (pro-inflammatory) macrophages was quantified using an antibody to iNOS. (C): The population of pro-tumorigenic (anti-inflammatory) macrophages was quantified with an antibody to CD206. Data for the whole tumors are shown as mean ± SEM ($n = 3$ for control samples; $n = 4$ for PEBCA and $n = 5$ for CBZ and PEBCA-CBZ). Asterisks indicate statistical significance obtained by unpaired parametric *t*-test, where $p < 0.0005$ is marked with *** and $p < 0.0001$ is marked with ****.

increased infiltration compared to the saline control only in tumors receiving PEBCA (Fig. 5C). Furthermore, the tumors of mice receiving PEBCA-CBZ showed significant lower levels (mean value of 23%) of this pro-tumorigenic macrophage population than tumors receiving PEBCA alone ($p < 0.001$; Fig. 5C).

3.6. In vitro cell studies

We tested cellular toxicity of PEBCA-CBZ, free CBZ and PEBCA without drug in three cell lines, specifically MDA-MB-231, MDA-MB-468 and MCF-7, measuring both cell proliferation by incorporation of [^{3}H]thymidine after 24 h and cell viability after 72 h by using the MTT assay. PEBCA-CBZ and CBZ were significantly more toxic than PEBCA without drug for all cell lines (range 130–350 fold), but there was no difference in the toxic effect of PEBCA-CBZ and CBZ in any of these test systems in any cell line (Fig. S5). It was also apparent that a small

fraction (10–20%) of the cells in all cell lines tested survived even very high CBZ concentrations when using the MTT assay after incubation for 72 h. The toxicity of PEBCA-CBZ and free CBZ were also tested in all three cell lines using two other test systems. The effect on protein synthesis (incorporation of [^{3}H]leucine) was measured following 24 h of incubation, and the ATP levels (CellTiter-Glo®) were measured after 72 h. The results obtained with these test systems (data not shown) were very similar to those shown in Fig. S5. The MTT assay was also performed on MDA-MB-231 cells after 24 and 48 h of incubation with similar results to those shown after 72 h of incubation (Fig. S5), although the toxic effect was smaller after these shorter incubation times (data not shown).

4. Discussion

The PEBCA NPs containing CBZ demonstrated a remarkable good therapeutic effect in the triple negative PDX mouse model, where complete remission was obtained in 6 out of 8 tumors following two injections of 15 mg CBZ/kg (Fig. 2A). Several possible explanations for the advantageous effect of PEBCA-CBZ versus free CBZ can be envisioned, and the obtained data point at least to the following factors: The longer circulation in blood and higher concentration of the drug in the tumor (Fig. 4) and the higher ratio of anti-tumorigenic (anti-iNOS labeled) macrophages to pro-tumorigenic (anti-CD206 labeled) macrophages [22,25] in the treated tumors (Fig. 5).

The quantification of CBZ in blood plasma clearly show a longer circulation time when the drug was incorporated in the NPs, with at least a 10-fold higher concentration in mice receiving PEBCA-CBZ compared free CBZ (Fig. 4A). When evaluating such data it is important to remember that the CBZ incorporated in NPs does not have a therapeutic effect before being released. Thus, release of the drug by diffusion and/or biodegradation of the NPs are necessary to obtain a good therapeutic effect as observed in the MAS98.12 model.

The in vivo fluorescence imaging data obtained with PEBCA NPs labeled with NR668 demonstrates accumulation of the fluorescence in the same tissues as those where CBZ was found to be present. As expected, these data show that most of the NPs ended up in the liver. The liver/spleen ratio of the fluorescence per pixel measured 24 h after injection was estimated to be 2.9 for NPs without CBZ and 2.4 for NPs with CBZ, whereas the ratio of total CBZ content in liver to spleen was calculated to 2.1 based on the MS analyses. Although one should be careful in interpreting the quantitative data from the fluorescent imaging (based upon per pixel measurements) the biodistribution data, obtained with two different methods, showed similar results. Our observations that injection of free NR668 did not give any measurable in vivo signal, the report that NR668 did not leak from NPs with a similar composition [26], and the different kinetics observed for PEBCA-CBZ and CBZ (Fig. 4A), indicate that most of the CBZ and NR668 are enclosed within the NPs 24 h after injection. Therefore, the biodistribution of these low molecular substances seems to represent well the distribution of the PEBCA NPs at this time point. In another study with comparable NPs, but using another PEGylation and fluorescent marker, a liver/spleen ratio of 5.3 was reported 6 h after injection [27]. In this study, the mean fluorescent signal obtained in the tumors 24 h after injection was 12% of that in liver for the NPs not containing CBZ and 3% for the NPs containing CBZ. The higher fluorescence obtained following injection of PEBCA NPs without drug than for NPs containing CBZ (Fig. 3A,B) may in part be due to the somewhat larger size of the NPs with drug (Table S1).

Macrophages are the most abundant immune cells in mammary tumors. Tumor associated macrophages (TAMs) were originally thought to exert anti-tumor activities, but increasing clinical and experimental evidence show that TAMs also may promote tumor progression and influence anticancer drug responses [28–30]. The pro-tumorigenic macrophages are known as alternatively activated and referred to as anti-inflammatory (M2-type), whereas the classically activated pro-inflammatory (M1-type) macrophages exhibit anti-tumorigenic properties [31,32]. Plasticity is a hallmark of the macrophage population and dynamic changes in their phenotype define the different subtypes [28]. A set of markers is usually recommended for a comprehensive characterization of the whole population [22,33]. In the present study we have used the well-accepted nitric oxide synthase (iNOS) for detection of the M1 phenotype and mannose receptor (CD206) to define the M2-type [22,33].

The TAMs are influenced by the context, e.g. by factors in the microenvironment or externally added anticancer drugs. Interestingly, the effect of docetaxel has been shown to partly depend upon depletion of M2 macrophages and expansion of M1 macrophages in models of breast cancer [34]. In contrast, we did not observe any response in the macrophage populations upon treatment with free CBZ, another taxane, despite efficient growth retardation. However, treatment with PEBCA encapsulated CBZ, resulted in significant improved anti-tumor efficacy, and complete remission in 75% of the tumors. Even though the number of tumors used for immunohistochemical quantification is small, our data suggest two possible mechanisms that might contribute to the good effect. First, a trend towards elevated inflammation in tumors upon treatment with PEBCA NPs (with or without drug) was observed. This may imply a role of PEBCA NPs in homing anti-tumorigenic M1 macrophages into the tumors, and thus further support the effect of CBZ. Secondly, we also showed that PEBCA-CBZ treatment significantly reduced CD206 expression in tumors compared to treatment with NPs without drug, which may point towards depletion of pro-tumorigenic macrophages.

Recently it was published that M2 macrophages show a vigorous endocytic uptake by macropinocytosis, whereas this uptake was virtually inactive in the M1 macrophages [35]. Furthermore, another study showed that the M2 macrophages use endocytosis to degrade collagen and promote tumor growth in solid tumors [36]. We speculate that the decrease in M2 macrophages observed after treatment with PEBCA-CBZ, and the concomitant pronounced effect on tumor growth, may be related to the macropinocytic uptake of PEBCA-CBZ and subsequent killing of these M2 macrophages. Thus, the inherent properties of M1 and M2 macrophages and selective toxic effect of drug containing particles on M2 macrophages may increase the efficacy of the treatment. It has earlier been published that driving TAMs towards M1 polarization (increasing the ratio of M1/M2 macrophages) has shown promising therapeutic effects in mice cancer models [36].

The effect of PEBCA-CBZ and free CBZ was also examined in orthotopically growing MDA-MB-231 tumors without showing the same efficacy as in the MAS98.12 PDX model. Since the influence of these NPs are based on the so-called EPR effect [3], the tumor vasculature is supposed to be a critical factor. We have earlier shown that the basal-like MAS98.12 tumor has a higher vascularization than the luminal-like MAS98.06 tumor [37,38]. Although angiogenesis also has been visualized in MDA-MB-231 tumors in mice [39], the difference in vascularization of the MAS98.12 and MDA-MB-231 tumors is less well characterized. However, in two previously published studies, the blood volume constituted 2.4% of the tumor volume 5 weeks after inoculation of MDA-MB-231 [39] and 5.9% at 5 weeks after transplantation of MAS98.12 [40], suggesting more efficient vascularization in the latter model.

Both the fluorescence in vivo imaging data and the quantification of CBZ in tissue samples clearly demonstrate accumulation of the PEBCA NPs in lymph nodes (Fig. 3B,C and Fig. 4B). Accumulation of drugs or imaging agents in lymph nodes was recently reviewed [41,42], suggesting a benefit of injecting very small NP [43,44]. A study reported accumulation into lymph nodes of particles similar to those used in the present study, i.e. poly(butylcyanoacrylate) modified with Pluronic F127 and loaded with vincristine [45]. As these NPs were shown to rapidly release vincristine and vincristine also accumulated in lymph nodes following injection of the non-encapsulated drug [45], it is difficult to evaluate to which extent these NPs actually accumulated in the

lymph nodes. Delivery of drug to lymph nodes has been discussed for treatment of metastasizing tumors [41,46]. Since local lymph nodes are the first site of breast cancer metastasis, and also a significant distant metastatic site, in particular in the aggressive triple negative basal like breast cancer [47], accumulation of PEBCA-CBZ in lymphatic tissue may be an important feature of such treatment.

In summary, the PEBCA-CBZ NPs seem promising for treatment of breast cancer, but further preclinical studies are necessary to show a beneficial effect of PEBCA-CBZ in metastatic cancer models. Furthermore, the observation that PEBCA seems to enhance intratumoral infiltration of anti-tumorigenic macrophages might be of general value and should be further investigated, either by using such NPs as an immune modulator or a vehicle able to enhance the therapeutic effect of encapsulated drugs.

Transparency declaration section

The authors declare potential conflict of interest through two pending patent applications.

Funding and acknowledgements

The two groups at Institute for Cancer Research and the group at SINTEF were all supported by the Research Council of Norway through its funding scheme NANO2021, project number 228200/O70 (Biodegradable nanoparticles in cancer diagnosis and therapy). The excellent technical assistance of Geir Frode Øy (animal studies), Tonje Sønstevold and Ane Sager Longva (cell studies), Anne Rein Hatletveit (particle synthesis) and Cathrine Løvmo (MS analyses) are greatly acknowledged. We thank the Department for Comparative Medicine for the services they provided and the other members of the NANOCAN project for valuable discussions.

Appendix A. Supplementary data

Supplementary data to this article can be found online at https://doi.org/10.1016/j.jconrel.2018.11.029.

References

[1] J. Shi, P.W. Kantoff, R. Wooster, O.C. Farokhzad, Cancer nanomedicine: progress, challenges and opportunities, Nat. Rev. Cancer 17 (1) (2017) 20–37.
[2] V.P. Torchilin, Multifunctional, stimuli-sensitive nanoparticulate systems for drug delivery, Nat. Rev. Drug Discov. 13 (11) (2014) 813–827.
[3] Y. Matsumura, H. Maeda, A new concept for macromolecular therapeutics in cancer chemotherapy: mechanism of tumoritropic accumulation of proteins and the antitumor agent smancs, Cancer Res. 46 (12) (1986) 6387–6392 Pt 1.
[4] U. Prabhakar, H. Maeda, R.K. Jain, E.M. Sevick-Muraca, W. Zamboni, O.C. Farokhzad, S.T. Barry, A. Gabizon, P. Grodzinski, D.C. Blakey, Challenges and key considerations of the enhanced permeability and retention effect for nanomedicine drug delivery in oncology, Cancer Res. 73 (8) (2013) 2412–2417.
[5] C. Vauthier, C. Dubernet, E. Fattal, H. Pinto-Alphandary, P. Couvreur, Poly(alkylcyanoacrylates) as biodegradable materials for biomedical applications, Adv. Drug Deliv. Rev. 55 (4) (2003) 519–548.
[6] E. Sulheim, H. Baghirov, H.E. Von, A. Boe, A.K. Aslund, Y. Morch, C.L. Davies, Cellular uptake and intracellular degradation of poly(alkyl cyanoacrylate) nanoparticles, J. Nanobiotechnol. 14 (2016) 1.
[7] E. Sulheim, T.G. Iversen, V. Nakstad, G. Klinkenberg, H. Sletta, R. Schmid, A.R. Hatletveit, A.M. Wagbo, A. Sundan, T. Skotland, K. Sandvig, Y. Morch, Cytotoxicity of Poly(Alkyl Cyanoacrylate) Nanoparticles, Int. J. Mol. Sci. 18 (2017) 2454.
[8] P. Vrignaud, D. Semiond, P. Lejeune, H. Bouchard, L. Calvet, C. Combeau, J.F. Riou, A. Commercon, F. Lavelle, M.C. Bissery, Preclinical antitumor activity of cabazitaxel, a semisynthetic taxane active in taxane-resistant tumors, Clin. Cancer Res. 19 (11) (2013) 2973–2983.
[9] C.J. Paller, E.S. Antonarakis, Cabazitaxel: a novel second-line treatment for metastatic castration-resistant prostate cancer, Drug Des. Devel. Ther. 5 (2011) 117–124.
[10] A.C. Mita, R. Figlin, M.M. Mita, Cabazitaxel: more than a new taxane for metastatic castrate-resistant prostate cancer? Clin. Cancer Res. 18 (24) (2012) 6574–6579.
[11] G.E. Duran, Y.C. Wang, E.B. Francisco, J.C. Rose, F.J. Martinez, J. Coller, D. Brassard, P. Vrignaud, B.I. Sikic, Mechanisms of resistance to cabazitaxel, Mol. Cancer Ther. 14 (1) (2015) 193–201.
[12] K. Knop, R. Hoogenboom, D. Fischer, U.S. Schubert, Poly(ethylene glycol) in drug delivery: pros and cons as well as potential alternatives, Angew. Chem. Int. Ed Engl 49 (36) (2010) 6288–6308.
[13] O. Engebraaten, H.K.M. Vollan, A.L. Borresen-Dale, Triple-negative breast cancer and the need for new therapeutic targets, Am. J. Pathol. 183 (4) (2013) 1064–1074.
[14] Z. Symon, A. Peyser, D. Tzemach, O. Lyass, E. Sucher, E. Shezen, A. Gabizon, Selective delivery of doxorubicin to patients with breast carcinoma metastases by stealth liposomes, Cancer 86 (1) (1999) 72–78.
[15] A. Gabizon, H. Shmeeda, Y. Barenholz, Pharmacokinetics of pegylated liposomal Doxorubicin: review of animal and human studies, Clin. Pharmacokinet. 42 (5) (2003) 419–436.
[16] E.M. Lindholm, A. Kristian, H. Nalwoga, K. Kruger, S. Nygard, L.A. Akslen, G.M. Maelandsmo, O. Engebraaten, Effect of antiangiogenic therapy on tumor growth, vasculature and kinase activity in basal- and luminal-like breast cancer xenografts, Mol. Oncol. 6 (4) (2012) 418–427.
[17] A.S.R. Klymchenko, N. Anton, H. Anton, I. Shulov, J. Vermot, Y. Mely, T.F. Vandamme, Highly lipophilic fluorescent dyes in nano-emulsions: towards bright non-leaking nano-droplets, RCS Advances 2 (2012) 11876–11886.
[18] D.L. Holliday, V. Speirs, Choosing the right cell line for breast cancer research, Breast Cancer Res. 13 (4) (2011) 215.
[19] A. Bergamaschi, G.O. Hjortland, T. Triulzi, T. Sorlie, H. Johnsen, A.H. Ree, H.G. Russnes, S. Tronnes, G.M. Maelandsmo, O. Fodstad, A.L. Borresen-Dale, O. Engebraaten, Molecular profiling and characterization of luminal-like and basal-like in vivo breast cancer xenograft models, Mol. Oncol. 3 (5–6) (2009) 469–482.
[20] W. Knapp, B. Dorken, P. Rieber, R.E. Schmidt, H. Stein, A.E. von Dem Borne, CD antigens 1989, Int. J. Cancer 44 (1) (1989) 190–191.
[21] W. Khazen, J. M'Bika, C. Tomkiewicz, C. Benelli, C. Chany, A. Achour, C. Forest, Expression of macrophage-selective markers in human and rodent adipocytes, FEBS Lett. 579 (25) (2005) 5631–5634.
[22] Y. Komohara, Y. Fujiwara, K. Ohnishi, M. Takeya, Tumor-associated macrophages: potential therapeutic targets for anti-cancer therapy, Adv. Drug Deliv. Rev. 99 (2016) 180–185 Pt B.
[23] Y.N. Blaker, M. Brodtkorb, J. Maddison, T.S. Hveem, J.A. Nesheim, H.M. Mohn, A. Kolstad, C.H. Geisler, K. Liestol, E.B. Smeland, H. Holte, J. Delabie, H. Danielsen, Computerized image analysis of the Ki-67 proliferation index in mantle cell lymphoma, Histopathology 67 (1) (2015) 62–69.
[24] B. Davies, T. Morris, Physiological parameters in laboratory animals and humans, Pharm. Res. 10 (7) (1993) 1093–1095.
[25] C.D. Mills, L.L. Lenz, R.A. Harris, A breakthrough: macrophage-directed cancer immunotherapy, Cancer Res. 76 (3) (2016) 513–516.
[26] S. Snipstad, S. Hak, H. Baghirov, E. Sulheim, Y. Morch, S. Lelu, E. von Haartman, M. Back, K.P.R. Nilsson, A.S. Klymchenko, C. de Lange Davies, A.K.O. Aslund, Labeling nanoparticles: Dye leakage and altered cellular uptake, Cytometry A 91 (8) (2017) 760–766.
[27] S. Snipstad, S. Berg, Y. Morch, A. Bjorkoy, E. Sulheim, R. Hansen, I. Grimstad, A. van Wamel, A.F. Maaland, S.H. Torp, C.L. Davies, Ultrasound Improves the delivery and therapeutic effect of nanoparticle-stabilized microbubbles in breast cancer xenografts, Ultrasound Med. Biol. 43 (11) (2017) 2651–2669.
[28] B.Z. Qian, J.W. Pollard, Macrophage diversity enhances tumor progression and metastasis, Cell 141 (1) (2010) 39–51.
[29] J. Condeelis, J.W. Pollard, Macrophages: obligate partners for tumor cell migration, invasion, and metastasis, Cell 124 (2) (2006) 263–266.
[30] B. Ruffell, L.M. Coussens, Macrophages and therapeutic resistance in cancer, Cancer Cell 27 (4) (2015) 462–472.
[31] A. Mantovani, A. Sica, M. Locati, Macrophage polarization comes of age, Immunity 23 (4) (2005) 344–346.
[32] Y. Komohara, M. Jinushi, M. Takeya, Clinical significance of macrophage heterogeneity in human malignant tumors, Cancer Sci. 105 (1) (2014) 1–8.
[33] A. Mantovani, A. Sica, S. Sozzani, P. Allavena, A. Vecchi, M. Locati, The chemokine system in diverse forms of macrophage activation and polarization, Trends Immunol. 25 (12) (2004) 677–686.
[34] K.N. Kodumudi, K. Woan, D.L. Gilvary, E. Sahakian, S. Wei, J.Y. Djeu, A novel chemoimmunomodulating property of docetaxel: suppression of myeloid-derived suppressor cells in tumor bearers, Clin. Cancer Res. 16 (18) (2010) 4583–4594.
[35] D.S. Redka, M. Gutschow, S. Grinstein, J. Canton, Differential ability of proinflammatory and anti-inflammatory macrophages to perform macropinocytosis, Mol. Biol. Cell 29 (1) (2018) 53–65.
[36] D.H. Madsen, H.J. Jurgensen, M.S. Siersbaek, D.E. Kuczek, L. Grey Cloud, S. Liu, N. Behrendt, L. Grontved, R. Weigert, T.H. Bugge, Tumor-associated macrophages derived from circulating inflammatory monocytes degrade collagen through cellular uptake, Cell Rep. 21 (13) (2017) 3662–3671.
[37] E.M. Huuse, S.A. Moestue, E.M. Lindholm, T.F. Bathen, H. Nalwoga, K. Kruger, A. Bofin, G.M. Maelandsmo, L.A. Akslen, O. Engebraaten, I.S. Gribbestad, In vivo MRI and histopathological assessment of tumor microenvironment in luminal-like and basal-like breast cancer xenografts, J. Magn. Reson. Imaging 35 (5) (2012) 1098–1107.
[38] A. Kristian, L.B. Nilsen, K. Roe, M.E. Revheim, O. Engebraten, G.M. Maelandsmo, R. Holm, E. Malinen, T. Seierstad, Dynamic (18) F-FDG PET for assessment of tumor physiology in two breast carcinoma xenografts, Nucl. Med. Mol. Imaging 47 (3) (2013) 173–180.
[39] J. Cebulla, E. Kim, K. Rhie, J. Zhang, A.P. Pathak, Multiscale and multi-modality visualization of angiogenesis in a human breast cancer model, Angiogenesis 17 (3) (2014) 695–709.
[40] E. Kim, H.M. Tunset, J. Cebulla, R. Vettukattil, H. Helgesen, A.J. Feuerherm, O. Engebraten, G.M. Maelandsmo, B. Johansen, S.A. Moestue, Anti-vascular effects of the cytosolic phospholipase A2 inhibitor AVX235 in a patient-derived basal-like breast cancer model, BMC Cancer 16 (2016) 191.

[41] X.Y. Zhang, W.Y. Lu, Recent advances in lymphatic targeted drug delivery system for tumor metastasis, Cancer Biol. Med. 11 (4) (2014) 247–254.
[42] F. Zhang, G. Niu, G. Lu, X. Chen, Preclinical lymphatic imaging, Mol. Imaging Biol. 13 (4) (2011) 599–612.
[43] Y.C. Tseng, Z. Xu, K. Guley, H. Yuan, L. Huang, Lipid-calcium phosphate nanoparticles for delivery to the lymphatic system and SPECT/CT imaging of lymph node metastases, Biomaterials 35 (16) (2014) 4688–4698.
[44] P. Kjellman, R. Zandt, S. Fredriksson, S.E. Strand, Optimizing retention of multimodal imaging nanostructures in sentinel lymph nodes by nanoscale size tailoring, Nanomedicine 10 (5) (2014) 1089–1095.
[45] R. Tan, M. Niu, J. Zhao, Y. Liu, N. Feng, Preparation of vincristine sulfate-loaded poly (butylcyanoacrylate) nanoparticles modified with pluronic F127 and evaluation of their lymphatic tissue targeting, J. Drug Target. 22 (6) (2014) 509–517.
[46] Y. Xie, T.R. Bagby, M.S. Cohen, M.L. Forrest, Drug delivery to the lymphatic system: importance in future cancer diagnosis and therapies, Expert Opin. Drug Deliv. 6 (8) (2009) 785–792.
[47] H. Kennecke, R. Yerushalmi, R. Woods, M.C. Cheang, D. Voduc, C.H. Speers, T.O. Nielsen, K. Gelmon, Metastatic behavior of breast cancer subtypes, J. Clin. Oncol. 28 (20) (2010) 3271–3277.